

“Design and Development of Angle of Attack Sensor”

*Master’s thesis submitted to*

Indian Institute of Technology Kharagpur

*in partial fulfillment of the requirements for the degree of*

Master of Technology

*in*

Aerospace Engineering

*by*

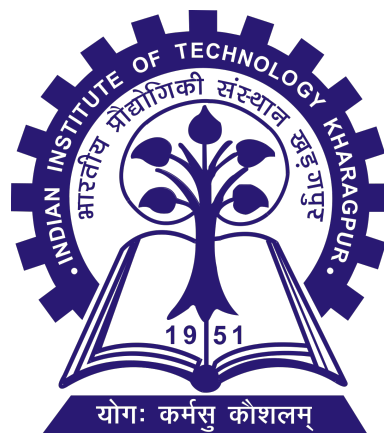
Satyam Choudhary  
20AE30047

*under supervision of*

Prof. Anup Ghosh

*and co-supervision of*

Prof. N. K. Peyada



Department of Aerospace Engineering  
Indian Institute of Technology Kharagpur  
Kharagpur, India  
Spring Semester, 2024 - 2025

## **Declaration**

---

I hereby declare that the work presented in this report titled “**Design and Development of Angle of Attack Sensor**” submitted to the Indian Institute of Technology Kharagpur, is an original contribution made by me under the guidance of Prof. Anup Ghosh and co-guidance of Prof. N. K. Peyada.

I affirm that:

- This thesis has not been submitted, either wholly or in part, to any other institution for any degree or diploma.
- The work has been carried out by me independently and all the sources of information have been duly acknowledged.
- I have adhered to the ethical standards and academic integrity guidelines set by the Institute.

**Satyam Choudhary**  
**20AE30047**  
**Kharagpur, May 2025**

## Acknowledgements

---

I extend my heartfelt gratitude to Prof. Anup Ghosh, my supervisor, for his invaluable guidance, unwavering support, and encouragement throughout this research. His expertise and mentorship have been instrumental in shaping the direction and success of this project.

I am equally indebted to Prof. N. K. Peyada, my co-supervisor, for his insightful feedback, constructive suggestions, and constant support. His commitment to academic excellence and attention to detail significantly enriched this study.

I would also like to express my appreciation to Mr. Nitin Pal for his insightful input and constructive feedback, which played a pivotal role in shaping the direction of this study.

I am also sincerely grateful to Mr. Nandi Rana, Mr. Sikdar Sandip, and Mr. Maity Bidyut for their valuable assistance and support during this project. Their readiness to share knowledge, offer technical insights, and help troubleshoot challenges made a significant difference in the successful completion of our work. I deeply appreciate their collaborative spirit, encouragement, and the many discussions that enriched both the learning process and the overall experience.

I am also deeply grateful to my friends and family for their steadfast support and understanding during this research journey. Their encouragement has been a source of strength, motivating me to persevere through challenges.

Finally, I would like to express my appreciation to the Department of Aerospace Engineering at IIT Kharagpur for providing the resources and environment necessary to undertake this research.

**Satyam Choudhary**  
**20AE30047**  
**Kharagpur, April 2025**

## Abstract

---

**Name of the student:** Satyam Choudhary

**Roll Number:** 20AE30047

**Degree for which submitted:** Masters of Technology

**Department:** Department of Aerospace Engineering

**Thesis Title:** Design and Development of Angle of Attack Sensor

**Thesis Supervisor:** Prof. Anup Ghosh

**Month and year of thesis submission:** May 2025

---

This study presents the design, development, and experimental validation of a high-resolution, lightweight Angle of Attack (AoA) sensor tailored for small-scale Unmanned Aerial Vehicles (UAVs) and aerodynamic research platforms. The sensor system integrates a Pro-Range 1024 PPR ABZ rotary encoder interfaced with a Raspberry Pi Pico 2W microcontroller, enabling real-time wireless angle measurement.

An aerodynamic fin, fabricated from balsa wood reinforced with fiberglass, is modeled considering aerodynamic, viscous, and inertial moments. Systematic wind tunnel tests at multiple airflow velocities were conducted to assess the sensor's dynamic response. Key performance parameters, such as natural frequency, damping ratio, and settling time, were extracted through time-resolved measurements and post-processing.

The sensor achieved angular resolution of  $0.088^\circ$ , damping ratios between 0.22–0.41, and response times under 0.5 seconds. The developed sensor demonstrated high sensitivity, fast stabilization, and robustness across the tested velocity ranges, making it suitable for integration into UAV platforms and for use in aerodynamic experimental studies.

Department of Aerospace Engineering  
Indian Institute of Technology Kharagpur  
Kharagpur, India



## Certificate

---

This is to certify that the work titled "**Design and Development of Angle of Attack Sensor**" has been carried out by **Satyam Choudhary** (Roll Number: **20AE30047**) under my supervision and co-supervision in partial fulfillment of the requirements for the award of the degree of **Master of Technology** in **Aerospace Engineering** at the **Indian Institute of Technology Kharagpur**.

---

**Prof. Anup Ghosh**

Department of Aerospace Engineering  
IIT Kharagpur  
2 May, 2025

**Prof. N. K. Peyada**

Department of Aerospace Engineering  
IIT Kharagpur  
2 May, 2025

# Contents

<b>1</b>	<b>Introduction</b>	<b>8</b>
<b>2</b>	<b>Literature Review</b>	<b>11</b>
2.1	Evolution of Angle of Attack Sensors . . . . .	11
2.2	Rotary Encoder-Based Sensing and Microcontroller Integration . . . . .	11
2.3	Advancements in Fin Materials and Mechanical Design . . . . .	12
2.4	Dynamic Characterization and Wind Tunnel Testing Practices . . . . .	12
2.5	Signal Processing, Noise Mitigation, and Data Integrity . . . . .	12
2.6	Summary . . . . .	12
<b>3</b>	<b>Objective</b>	<b>14</b>
<b>4</b>	<b>Theoretical Background</b>	<b>15</b>
4.1	Principles of High-Resolution Rotary Encoder-Based Angle Measurement	15
4.2	Aerodynamic Moment Balance and System Modeling . . . . .	16
4.3	Dynamic System Behavior and Parameters . . . . .	18
4.3.1	Natural Frequency . . . . .	18
4.3.2	Damping Ratio . . . . .	19
4.4	Wind Tunnel Testing Methodology . . . . .	19
<b>5</b>	<b>Methodology</b>	<b>20</b>
5.1	Design and System Integration . . . . .	20
5.2	Microcontroller Programming . . . . .	23
5.3	Circuit Fabrication and Hardware Assembly . . . . .	24
5.4	Mechanical Fabrication: Fin and Mounting Structure . . . . .	27
5.4.1	Fabrication of the Aerodynamic Fin . . . . .	27
5.4.2	Fin-Encoder Coupling . . . . .	29
5.4.3	Mounting in Wind Tunnel . . . . .	29
5.5	Wind Tunnel Testing Procedure . . . . .	31
5.6	Data Acquisition and Recording . . . . .	31
5.7	Post-Processing and Data Analysis . . . . .	32

<b>6 Results and Discussion</b>	<b>34</b>
6.1 Experimental Conditions and Data Acquisition . . . . .	34
6.2 Time versus Angular Displacement Plots . . . . .	34
6.2.1 Response at 700 rpm (15.5 m/s) . . . . .	35
6.2.2 Response at 800 rpm (16.2 m/s) . . . . .	36
6.2.3 Response at 1000 rpm (20.73 m/s) . . . . .	37
6.2.4 Comparison between Simulated and Experimental Results . . . . .	38
6.3 Calculation of Damping Ratio and Natural Frequency . . . . .	40
6.3.1 Settling Time Analysis . . . . .	40
6.4 Effect of Initial Deflection Angle . . . . .	41
6.5 Summary of Extracted Parameters . . . . .	41
6.6 Comparison with Literature . . . . .	42
6.7 Sources of Experimental Error and Limitations . . . . .	42
<b>7 Conclusion</b>	<b>44</b>

# 1 Introduction

The increasing deployment of unmanned aerial vehicles (UAVs) in civil, military, and research applications has intensified the demand for lightweight, compact, and reliable sensing systems capable of real-time flight parameter monitoring. Among various aerodynamic parameters, the Angle of Attack (AoA) is of critical importance for UAV flight stability, maneuverability, and performance optimization.

The AoA, defined as the angle between the chord line of the wing and the oncoming airflow, has a direct influence on lift generation, stall onset, and overall aerodynamic efficiency. Precise knowledge of AoA enables enhanced control algorithms, improved stall warning systems, and better flight envelope protection, particularly in lightweight UAV platforms operating under dynamic flight conditions.

$$\alpha = \arctan \left( \frac{V_z}{V_x} \right) \quad (1)$$

where  $V_z$  is the vertical velocity component and  $V_x$  is the horizontal velocity component along the chord.

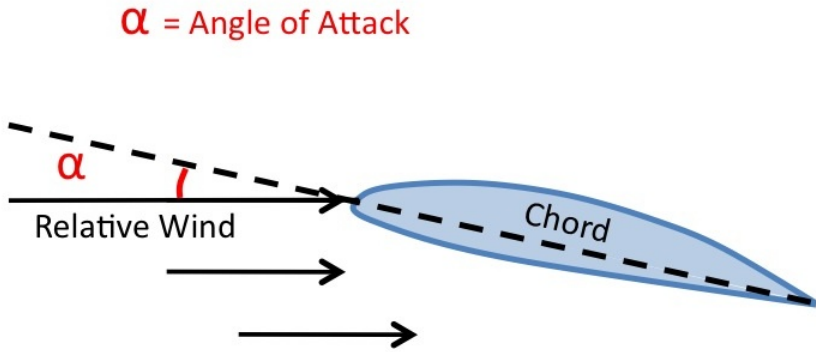


Figure 1: Definition of Angle of Attack ( $\alpha$ ) between chord line and relative airflow

Traditionally, AoA sensors employed mechanical systems such as vanes or differential pressure probes. However, these systems often suffered from limited dynamic response and were unsuitable for small UAVs due to added weight and complexity. Recent advancements in microcontroller-based systems, lightweight materials, and wireless technologies have enabled the development of more efficient AoA sensors.

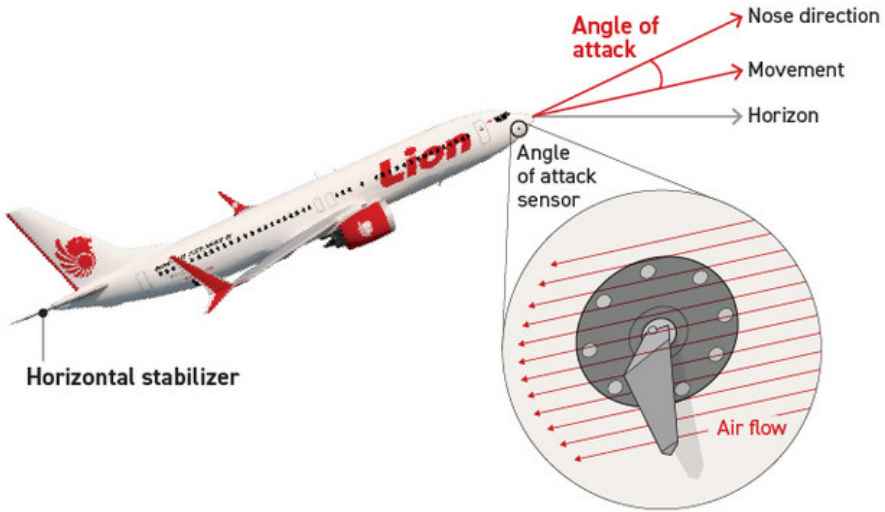


Figure 2: Location and type of AoA sensors used in civil Aircrafts

In this project, the focus is on developing a compact and high-resolution Angle of Attack sensor specifically designed for small UAV platforms. The sensor integrates:

- A Raspberry Pi Pico 2W microcontroller platform featuring dual-core Cortex-M33 processors and onboard wireless capability,
- A Pro-Range 1024 Pulses Per Revolution (PPR) ABZ 3-phase rotary encoder for precise angular measurement,
- A lightweight aerodynamic fin made from balsa wood reinforced with fiberglass to achieve high stiffness-to-weight ratio,
- A 16-pin LCD module for real-time display during ground testing and calibration,
- A Veroboard-mounted compact circuit integrated inside a balsa wood protective box to minimize aerodynamic disturbances.

The sensor assembly was mounted on a custom-fabricated structure inspired by the Wright-Patterson Vane Assembly principles to ensure robust alignment with airflow. Testing was performed inside a low-speed wind tunnel across different fan rotational speeds corresponding to airflow velocities of 15.5 m/s (700 rpm), 16.2 m/s (800 rpm), and 20.73 m/s (1000 rpm).

The key performance parameters such as damping ratio, natural frequency, and settling time were determined from the dynamic response of the vane under varying airflow conditions. Experimental data were acquired using a Python-based acquisition system.

This development offers a cost-effective and reliable solution for high-fidelity AoA sensing in aerodynamic research and lightweight UAV applications.

## 2 Literature Review

The measurement of Angle of Attack (AoA) is a crucial aspect in aerodynamic research, UAV flight dynamics, and atmospheric studies. Over the decades, various types of AoA sensors have been developed and tested, starting from simple mechanical vanes to high-resolution electronic sensors. A brief review of related works relevant to the present development is discussed below.

### 2.1 Evolution of Angle of Attack Sensors

Initially, AoA measurements were carried out using mechanical vanes, commonly referred to as wind vanes. These devices were simple in construction but suffered from low dynamic response due to mechanical inertia and friction. Barna and Crossman systematically investigated the aerodynamic performance and dynamic response of flow direction sensing vanes, including flat plates, cruciforms, bi-vanes, and box-type vanes. Their work showed that vane planform geometry and aspect ratio have significant influence on damping, natural frequency, and overall sensor responsiveness.

Later, Karam developed a comprehensive dynamic model of AoA vane assemblies, considering aerodynamic, inertial, and frictional moments. The Wright-Patterson Vane Assembly, designed based on these principles, demonstrated improved dynamic characteristics and has since been widely referenced in vane sensor design.

### 2.2 Rotary Encoder-Based Sensing and Microcontroller Integration

With advancements in electronics, rotary encoders became an attractive solution for AoA measurement. Zadirienko et al. demonstrated an Arduino-based AoA sensor using an incremental rotary encoder. Their design offered high accuracy at low cost, with real-time angle tracking.

Further, Wanngoen et al. implemented high-resolution magnetic rotary encoders for small UAVs, achieving angular resolutions as fine as  $0.06^\circ$ . These works underline the importance of microcontroller platforms such as Arduino and Raspberry Pi for real-time data acquisition and wireless telemetry in aerodynamic sensing applications.

## **2.3 Advancements in Fin Materials and Mechanical Design**

The dynamic response of an AoA sensor is heavily dependent on the mass moment of inertia of its fin assembly. Traditional aluminum fins, although structurally rigid, led to poor dynamic behavior due to their higher inertia. As a result, lightweight materials like balsa wood reinforced with fiberglass became popular, offering an excellent stiffness-to-weight ratio. Such designs ensure higher natural frequencies, improved damping, and reduced steady-state oscillations during airflow perturbations.

## **2.4 Dynamic Characterization and Wind Tunnel Testing Practices**

Karam emphasized that for an AoA vane to respond accurately to rapid flow changes, its natural frequency must be sufficiently high, and damping must be moderate. Wind tunnel experiments by Barna and Crossman validated the theoretical models by measuring vane dynamic response under varying flow conditions and Reynolds numbers. Standard testing practices include static calibration of angle response, free decay oscillation measurements, and dynamic characterization through time-history analysis.

## **2.5 Signal Processing, Noise Mitigation, and Data Integrity**

Modern AoA sensing systems incorporate advanced signal processing techniques to improve reliability. Use of quadrature decoding for encoder outputs, software debouncing, low-pass filtering, and real-time wireless data transmission ensure accurate angle measurement even under vibration-prone environments like wind tunnels or UAV flights.

These techniques, combined with high-frequency data acquisition systems, enable the extraction of dynamic parameters like damping ratio, natural frequency, and settling time with high accuracy.

## **2.6 Summary**

The literature review highlights the evolution of AoA sensors from simple mechanical vanes to sophisticated microcontroller-based wireless systems. The present work

draws inspiration from the Wright-Patterson Vane Assembly, Barna and Crossman's dynamic characterization studies, and modern practices in rotary encoder interfacing, to develop a lightweight, wireless, high-resolution AoA sensor optimized for small UAV applications.

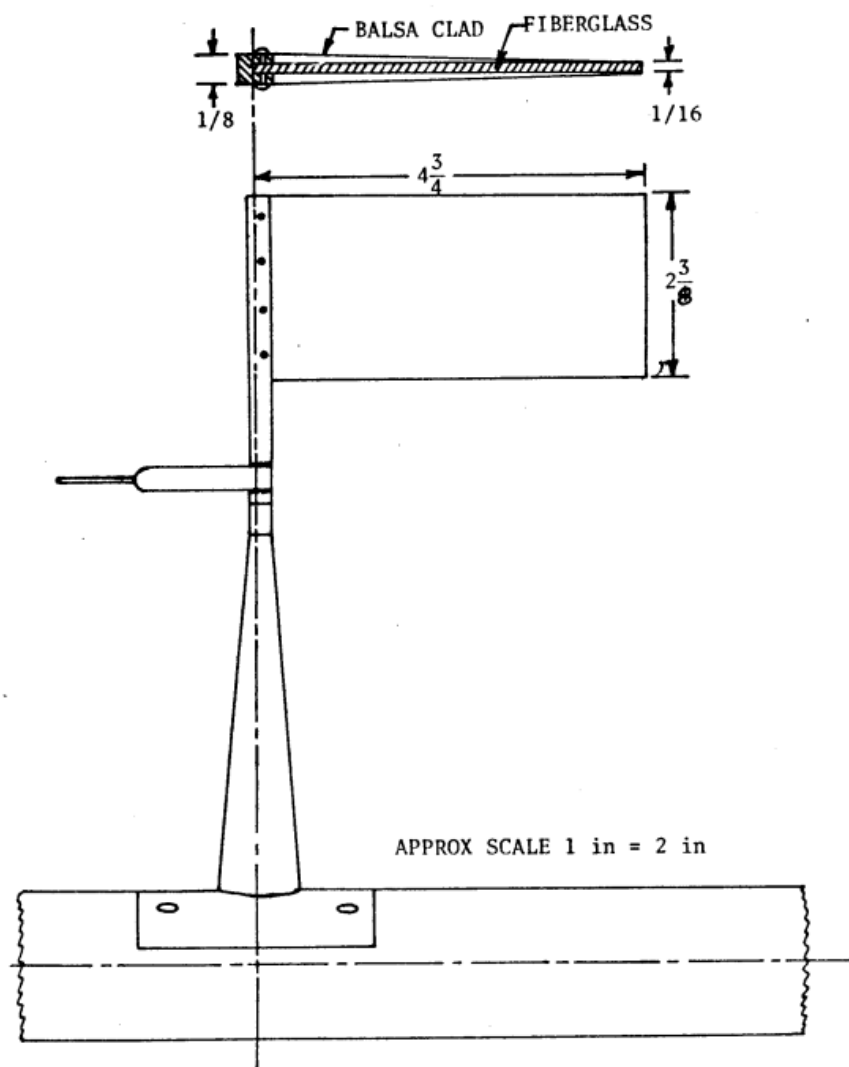


Figure 3: Geometric representation of the Wright-Patterson vane assembly configuration (Source[2])

### **3 Objective**

The objective of this project is to design, develop, and test an Angle of Attack (AoA) sensor system that is lightweight, compact, and accurate, making it suitable for small unmanned aerial vehicles (UAVs) and aerodynamic research.

The specific goals are:

1. To build a microcontroller-based system using the Raspberry Pi Pico 2W and a high-resolution 1024 PPR rotary encoder for real-time angle measurement.
2. To create a lightweight aerodynamic fin from balsa wood reinforced with fiber-glass, coupled with the encoder for accurate airflow direction sensing.
3. To assemble the complete system, including LCD display and electronics, into a compact and durable enclosure.
4. To develop a Python-based data acquisition system for logging and processing sensor data.
5. To conduct systematic wind tunnel experiments at different flow velocities to study the dynamic response, including damping, natural frequency, and settling behavior.

This project aims to deliver a reliable and precise Angle of Attack sensor for UAV and wind tunnel applications.

## 4 Theoretical Background

This section explores the theoretical principles underlying the design, operation, and testing of the Angle of Attack (AoA) sensor developed in this project. It covers the working of the rotary encoder for angular measurement, the moment balance in aerodynamic systems, and the dynamic behavior of the vane assembly.

### 4.1 Principles of High-Resolution Rotary Encoder-Based Angle Measurement

Rotary encoders are high-precision devices used to measure angular displacement by converting mechanical rotation into digital signals. In this project, a Pro-Range 1024 Pulses Per Revolution (PPR) ABZ 3-phase incremental rotary encoder was employed.

The encoder generates two quadrature outputs (Channel A and Channel B), which are 90 degrees out of phase. By counting the pulses and monitoring the phase sequence, the direction and magnitude of rotation can be determined.

The total number of counts per revolution (CPR) is calculated as:

$$\text{CPR} = 4 \times \text{PPR} \quad (2)$$

Thus, for the Pro-Range 1024 PPR encoder:

$$\text{CPR} = 4096 \text{ counts/rev}$$

The angular resolution achieved is:

$$\theta_{\text{resolution}} = \frac{360^\circ}{4096} \approx 0.088^\circ \quad (3)$$

An interrupt-based counting method was implemented on the Raspberry Pi Pico 2W microcontroller to accurately track the encoder signals and compute the angular position. Debounce filtering and glitch suppression algorithms were incorporated in the firmware to ensure robust signal acquisition under vibratory conditions.

## 4.2 Aerodynamic Moment Balance and System Modeling

The vane operates based on a moment balance about the pivot axis, involving aerodynamic, viscous, and inertial moments. The overall equilibrium condition is given by:

$$\sum M = M_{\text{aero}} + M_{\text{viscous}} + M_{\text{inertial}} = 0 \quad (4)$$

Where:

- $M_{\text{aero}}$  = aerodynamic restoring moment,
- $M_{\text{viscous}}$  = damping moment opposing angular velocity,
- $M_{\text{inertial}}$  = inertial moment opposing angular acceleration.

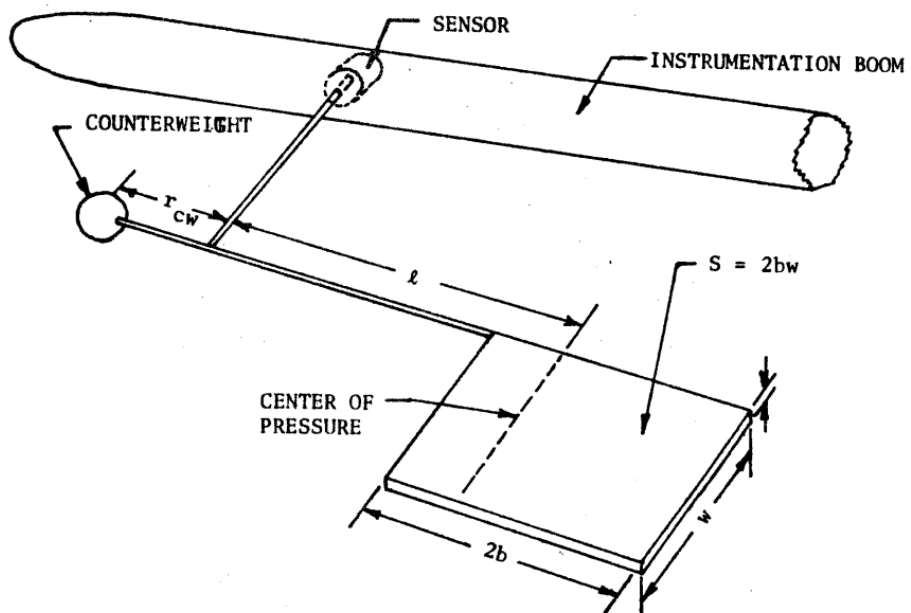


Figure 4: Configuration of an Idealized AoA sensor vane (Source[2])

Figure 4 represents an idealized wind vane. A flat plate with a smoothed leading edge mounted on a long slender arm attended with a movable mass on the other side of the arm pivoted by the contactless potentiometer. This system is mounted on a wind tunnel instrumentation boom. A counterweight is provided so that the vane assembly is statically balanced.

The aerodynamic lift force acting on the fin is expressed as:

$$L = \frac{1}{2} \rho u^2 S C_L \quad (5)$$

where:

- $\rho$  = air density,
- $u$  = free-stream velocity,
- $S$  = surface area of the fin,
- $C_L$  = lift coefficient of the fin, assumed to be linear with angle  $\alpha$  for small deflections.

The aerodynamic moment about the pivot is:

$$M_{\text{aero}} = L \times d_{\text{aero}} \quad (6)$$

where  $d_{\text{aero}}$  is the distance from the pivot to the aerodynamic center (typically 25% chord length).

The viscous damping moment is modeled as:

$$M_{\text{viscous}} = -B\dot{\theta} \quad (7)$$

where  $B$  is the damping coefficient and  $\dot{\theta}$  is the angular velocity.

The inertial moment is:

$$M_{\text{inertial}} = -J\ddot{\theta} \quad (8)$$

where  $J$  is the mass moment of inertia of the vane assembly and  $\ddot{\theta}$  is the angular acceleration.

Combining all, the dynamic equation of motion becomes:

$$J\ddot{\theta} + B\dot{\theta} + K_{\text{aero}}\theta = 0 \quad (9)$$

where  $K_{\text{aero}}$  represents the aerodynamic stiffness given by:

$$K_{\text{aero}} = \frac{1}{2}\rho u^2 S a d_{\text{aero}} \quad (10)$$

Here,  $a$  is the lift-curve slope ( $dC_L/d\alpha$ ).

### 4.3 Dynamic System Behavior and Parameters

The dynamic behavior of the vane resembles that of a damped harmonic oscillator. Important parameters are defined as:

#### 4.3.1 Natural Frequency

The natural frequency  $f_n$  is given by:

$$f_n = \frac{1}{2\pi} \sqrt{\frac{K_{\text{aero}}}{J}} \quad (11)$$

Higher natural frequency indicates faster system response.

#### 4.3.2 Damping Ratio

The damping ratio  $\zeta$  is calculated as:

$$\zeta = \frac{B}{2\sqrt{JK_{\text{aero}}}} \quad (12)$$

A moderate damping ratio (0.2–0.5) ensures a balance between stability and quick response.

### 4.4 Wind Tunnel Testing Methodology

Wind tunnel experiments were conducted to validate the theoretical predictions. The free-stream velocity was determined using Bernoulli's principle:

$$\Delta P = \frac{1}{2} \rho u^2 \quad (13)$$

where  $\Delta P$  is the pressure differential measured inside the tunnel.

Testing was performed at three fan rotational speeds, corresponding to velocities:

- 700 rpm → 15.5 m/s,
- 800 rpm → 16.2 m/s,
- 1000 rpm → 20.73 m/s.

The vane was initially displaced by a known angle and released to undergo free-decay oscillations. The time vs angle response was recorded, and the damping ratio and natural frequency were calculated accordingly.

## 5 Methodology

This section describes in detail the systematic approach adopted for the design, fabrication, coding, experimental setup, data acquisition, and analysis of the developed Angle of Attack (AoA) sensor.

### 5.1 Design and System Integration

The sensor system was designed to provide high-resolution angular measurements. Although the Raspberry Pi Pico 2W supports wireless communication, all data logging was performed over USB due to integration issues with the Wi-Fi module.

Key components integrated in the system included:

- A Pro-Range 1024 Pulses Per Revolution (PPR) ABZ 3-phase rotary encoder for precise angular position sensing,



Figure 5: Pro-Range 1024 PPR ABZ 3-phase incremental rotary encoder used for angular sensing

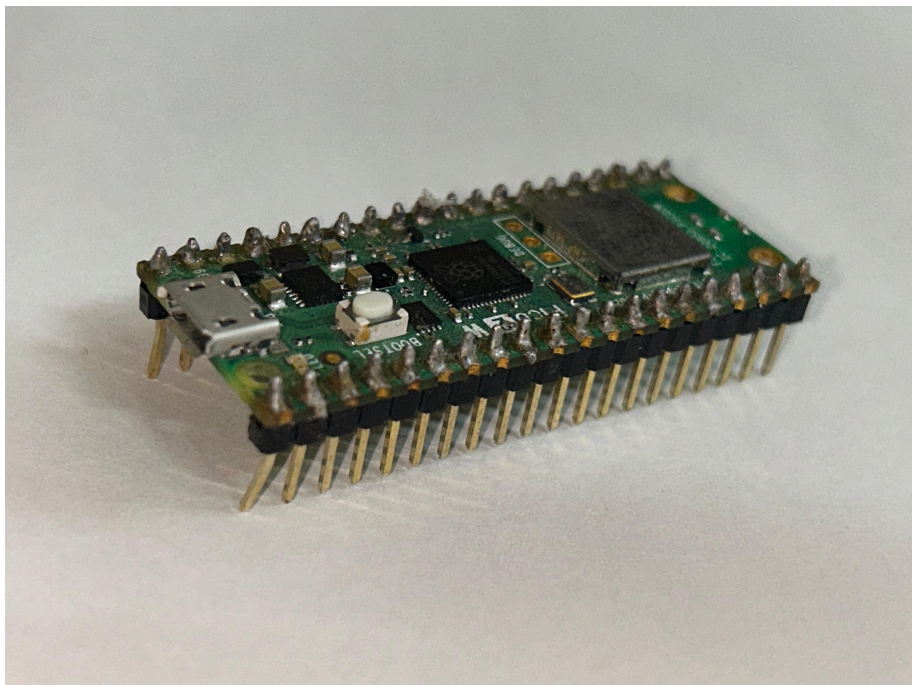


Figure 6: Raspberry Pi Pico 2W microcontroller

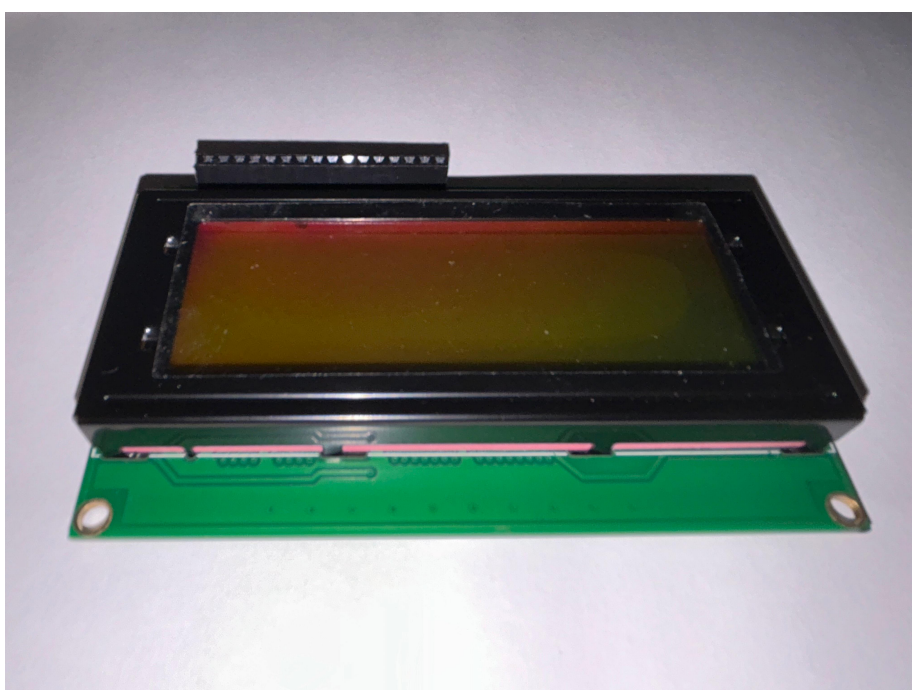
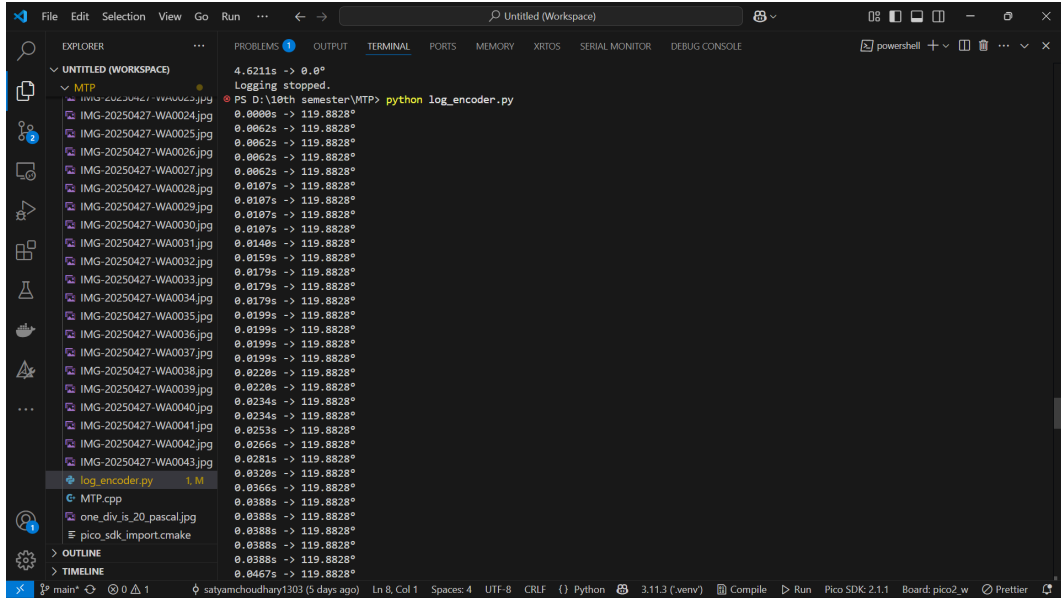


Figure 7: 16-pin LCD display module

- A Raspberry Pi Pico 2W microcontroller platform, featuring dual-core Cortex-M33 processors and onboard Wi-Fi,
- A 16-pin LCD display module for real-time visualization of the angle readings,
- A Python-based data acquisition setup,



The screenshot shows a terminal window titled "Untitled (Workspace)" with the following content:

```

4.6211s -> 0.0°
Logging stopped.

PS D:\10th semester\MP> python log_encoder.py
0.0000s -> 119.8828°
0.0062s -> 119.8828°
0.0107s -> 119.8828°
0.0107s -> 119.8828°
0.0107s -> 119.8828°
0.0107s -> 119.8828°
0.0140s -> 119.8828°
0.0159s -> 119.8828°
0.0179s -> 119.8828°
0.0179s -> 119.8828°
0.0179s -> 119.8828°
0.0199s -> 119.8828°
0.0199s -> 119.8828°
0.0199s -> 119.8828°
0.0199s -> 119.8828°
0.0228s -> 119.8828°
0.0228s -> 119.8828°
0.0234s -> 119.8828°
0.0234s -> 119.8828°
0.0253s -> 119.8828°
0.0256s -> 119.8828°
0.0281s -> 119.8828°
0.0320s -> 119.8828°
0.0366s -> 119.8828°
0.0388s -> 119.8828°
0.0388s -> 119.8828°
0.0388s -> 119.8828°
0.0388s -> 119.8828°
0.0467s -> 119.8828°

```

The terminal also shows the file structure of the workspace, including Python scripts like `log_encoder.py`, C/C++ files like `MTP.cpp`, and images like `one_div_is_20_pascal.jpg`.

Figure 8: Terminal output displaying encoder-derived angular displacement values in real time

- A lightweight aerodynamic fin fabricated using balsa wood reinforced with a fiberglass layer. The fin had dimensions: chord = 6 cm, span = 12 cm.

The complete system was designed for compactness, minimal inertia, and operational robustness suitable for wind tunnel testing environments. The overall setup, including the soldered circuit, was enclosed within a hand-crafted balsa wood box for protection.

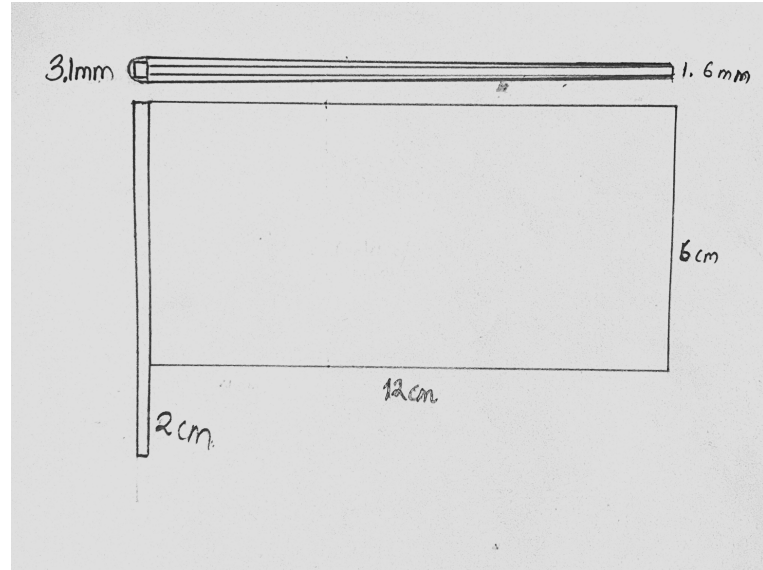


Figure 9: Final aerodynamic fin design and dimensions

## 5.2 Microcontroller Programming

The encoder outputs two quadrature signals (Channel A and Channel B), which were connected to the GPIO pins of the Raspberry Pi Pico 2W. The firmware was developed in C++ using VS Code.

The programming workflow included:

- Configuring GPIO interrupts to detect rising and falling edges,
- Pulse counting and direction determination,
- Real-time angle computation using:

$$\theta = \left( \frac{\text{Pulse Count}}{4096} \right) \times 360^\circ$$

- Displaying the angle on LCD and sending the data over USB serial connection to the ground station.



Figure 10: Fully enclosed AoA sensor unit showing encoder, shaft, and display integrated into the protective housing

### 5.3 Circuit Fabrication and Hardware Assembly

The entire sensor circuit—including the Raspberry Pi Pico 2W, 1024 PPR rotary encoder, LCD module, pull-up resistors, and power supply wiring—was assembled on a compact Veroboard setup. The Raspberry Pi Pico served as the microcontroller unit for signal acquisition, processing, and display. The LCD display was programmed to show real-time angle readings, while the encoder outputs were read using GPIO interrupts.

The following figures provide a detailed schematic of the hardware integration:

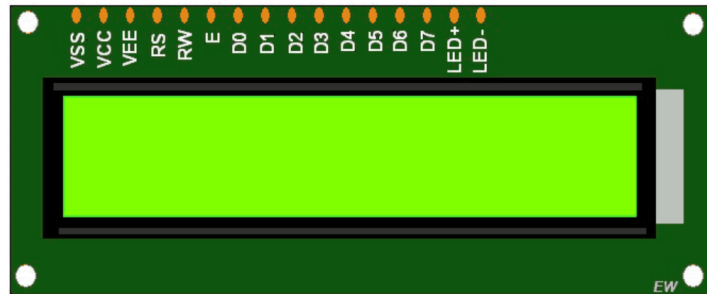


Figure 11: Pinout configuration of the 16-pin character LCD display used for real-time output

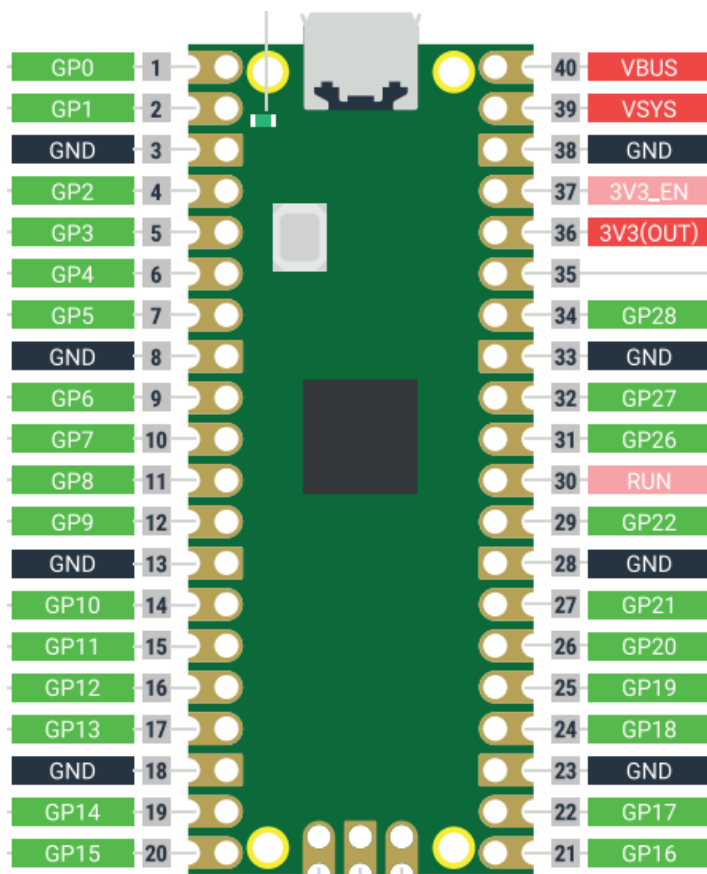


Figure 12: Pin mapping of Raspberry Pi Pico 2W showing 40 GPIO pins and relevant power lines

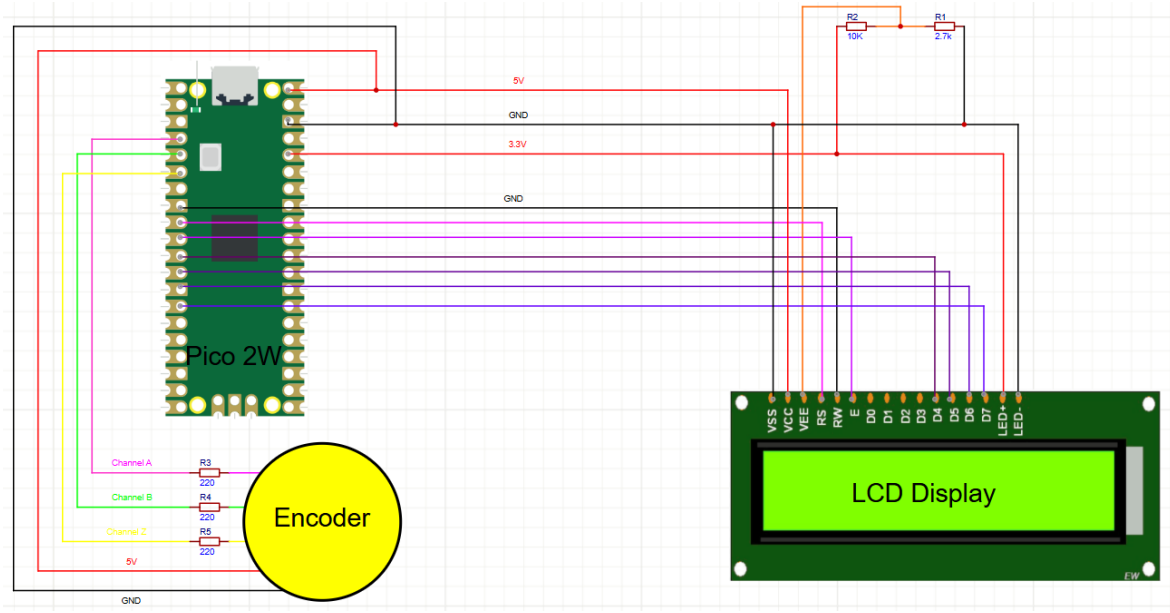


Figure 13: Complete schematic diagram showing interconnections between Raspberry Pi Pico 2W, rotary encoder, and LCD display with supporting resistors

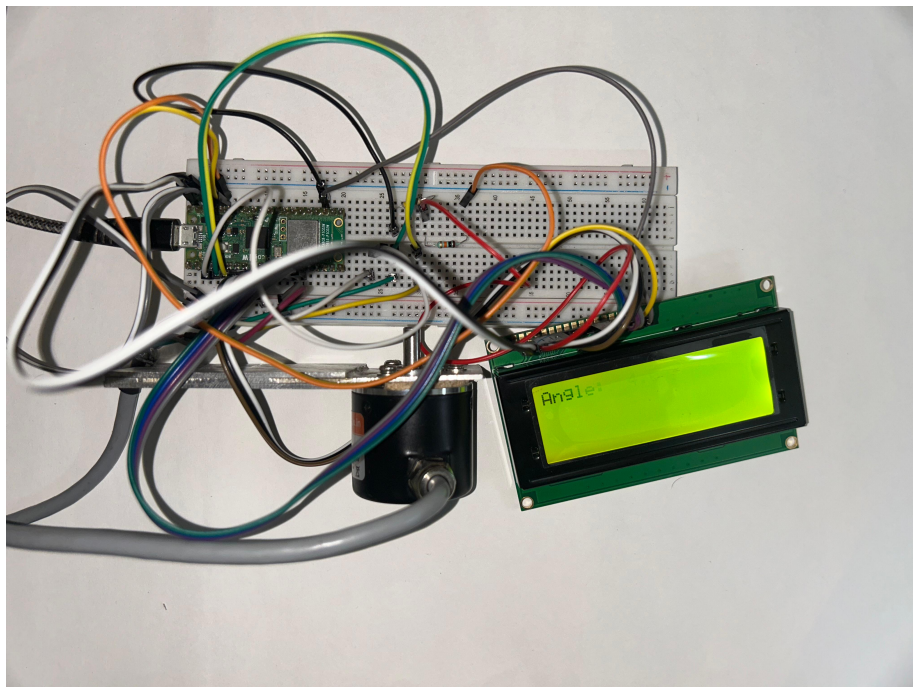


Figure 14: Complete circuit including LCD, encoder connections, and microcontroller for windtunnel testing

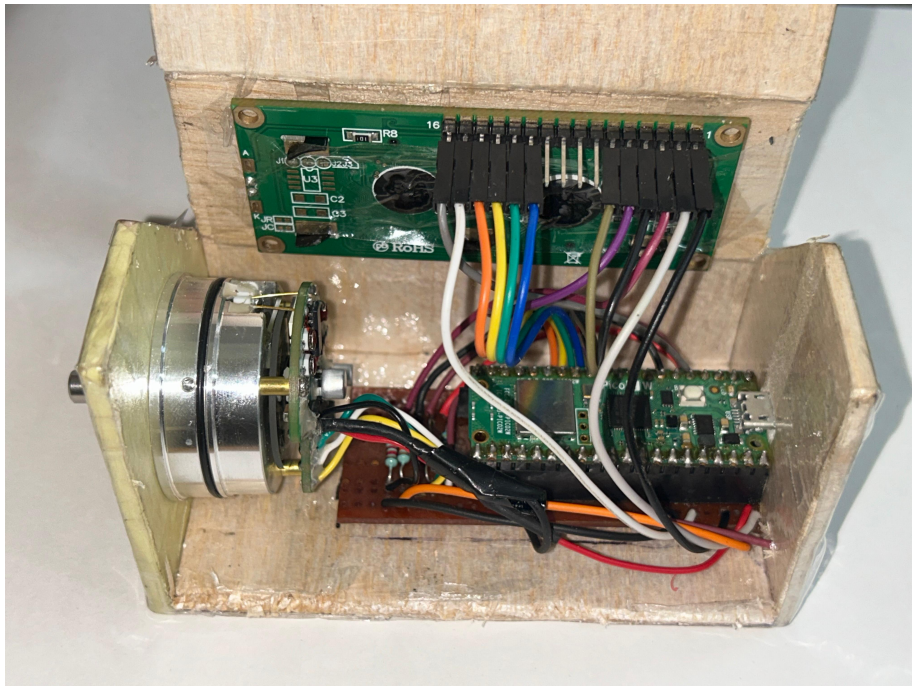


Figure 15: Fabricated Veroboard circuit containing all electronics compactly assembled

## 5.4 Mechanical Fabrication: Fin and Mounting Structure

### 5.4.1 Fabrication of the Aerodynamic Fin

The aerodynamic fin was crafted using lightweight balsa wood reinforced with fiberglass to enhance structural stiffness while maintaining minimal weight. Fin specifications:

- **Material:** Balsa wood with fiberglass skin.
- **Span:** 6 cm.
- **Chord length:** 12 cm.
- **Leading edge thickness:** 3 mm.
- **Trailing edge thickness:** 1.6 mm.
- **Mass of fin:** 10 grams.
- **Surface finish:** Finished with sand paper to minimize surface roughness.

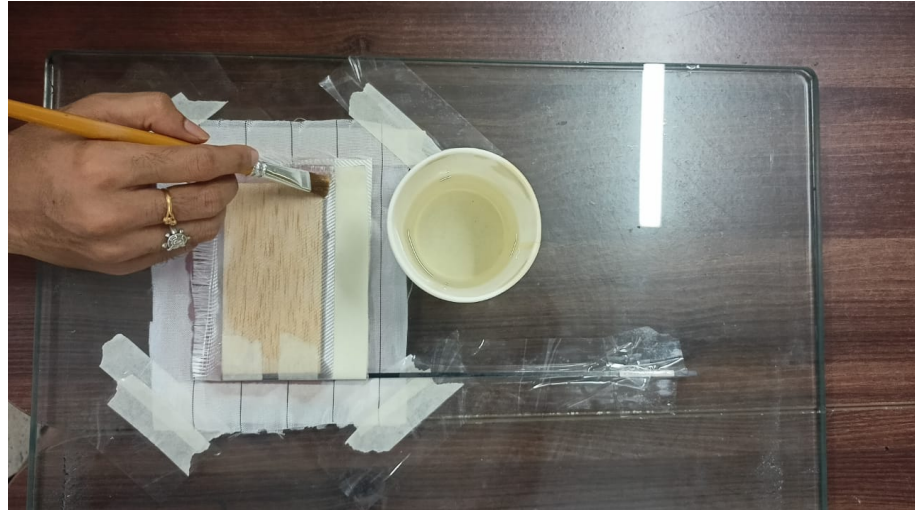


Figure 16: Application of epoxy over fiberglass-reinforced balsa fin for added strength and surface finish



Figure 17: Final fabricated aerodynamic fin with encoder shaft connection for precise angular transmission

### 5.4.2 Fin-Encoder Coupling

The fin was mechanically coupled to the encoder shaft using a custom-fabricated connector, ensuring rigid attachment and precise transfer of aerodynamic deflection.



Figure 18: Custom fabricated coupling used to rigidly attach fin to rotary encoder shaft

### 5.4.3 Mounting in Wind Tunnel

The assembled AoA sensor was mounted on a horizontal arm inspired by the Wright Patterson Vane Assembly configuration for wind tunnel tests.

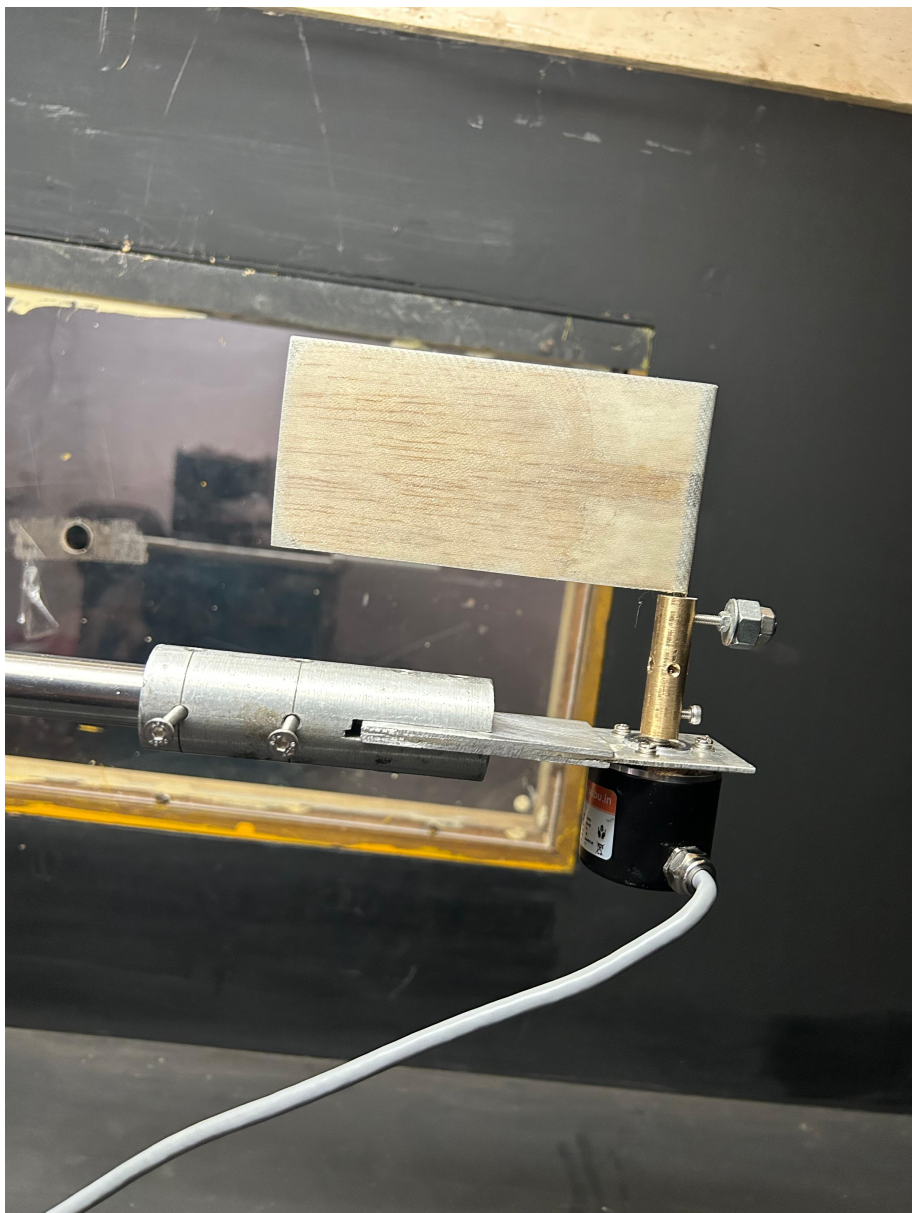


Figure 19: Wind Tunnel Setup with Wright Patterson Inspired Mounting

## 5.5 Wind Tunnel Testing Procedure

Wind tunnel experiments were conducted at the following controlled free-stream velocities:

- 700 rpm → 15.5 m/s
- 800 rpm → 16.2 m/s
- 1000 rpm → 20.73 m/s

Testing protocol:

1. Manually deflect the fin to known angles ( $10^\circ$ ,  $20^\circ$ ,  $30^\circ$ ,  $45^\circ$ ),
2. Stabilize tunnel speed,
3. Release the fin and record the free-decay oscillations.

Multiple repetitions were performed to ensure statistical consistency.

## 5.6 Data Acquisition and Recording

The angular data was streamed via USB and logged using a Python script with timestamping. Data sampling frequency was optimized to capture oscillation dynamics.

Each dataset contained:

- Time (seconds),
- Angular Position (degrees).

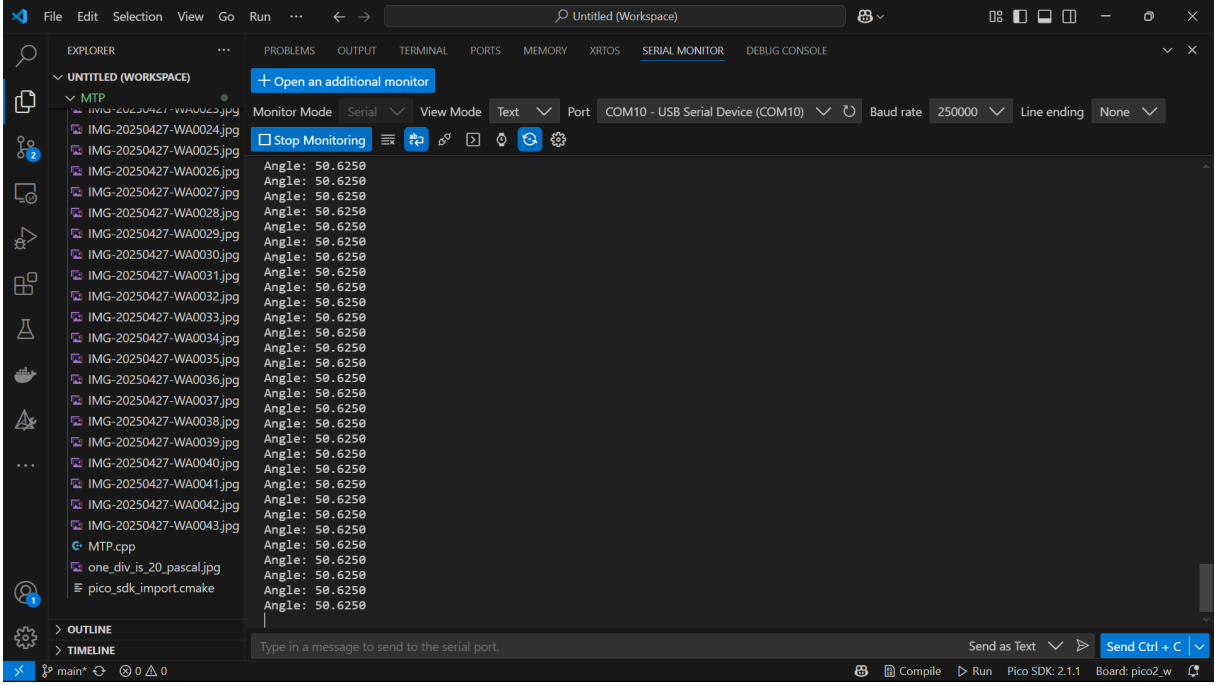


Figure 20: Serial monitor output showing real-time angular data acquisition and transmission

## 5.7 Post-Processing and Data Analysis

- Plotting angular displacement vs time,
- Calculating logarithmic decrement ( $\delta$ ),
- Estimating damping ratio ( $\zeta$ ) using:

$$\zeta = \frac{\delta}{\sqrt{4\pi^2 + \delta^2}}$$

- Calculating natural frequency ( $f_n$ ) from the oscillation period:

$$f_n = \frac{1}{T}$$

- Estimating settling time to reach within 5% of final position.

These analyses provided insights into the dynamic behavior and performance validation of the developed AoA sensor.

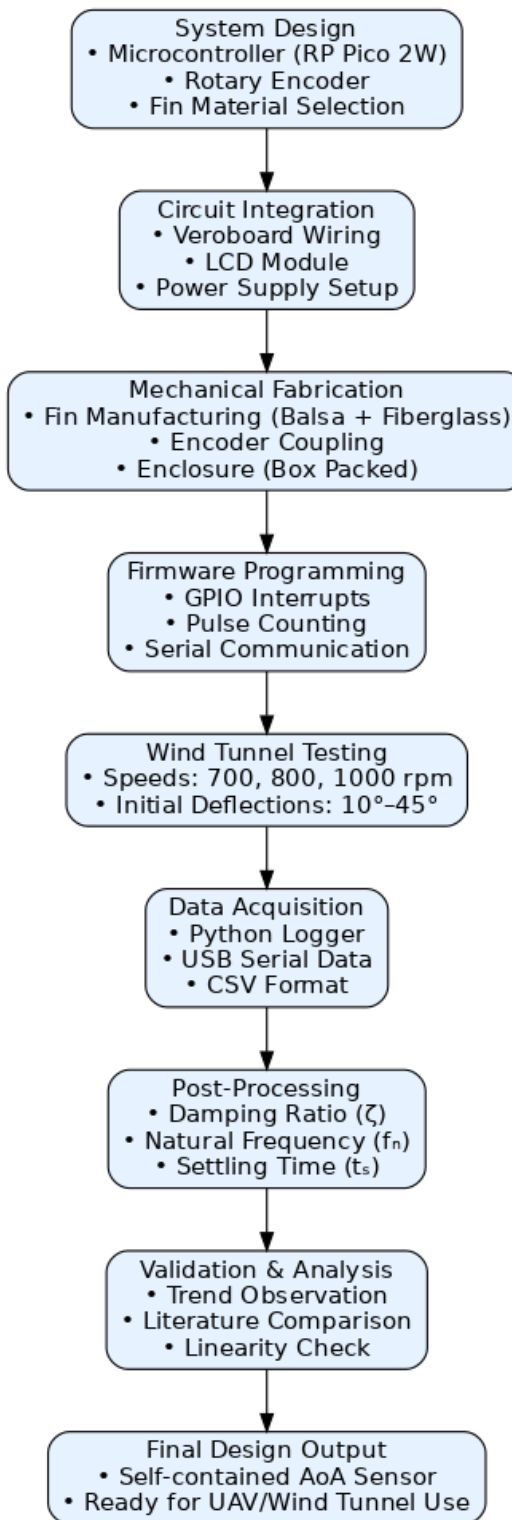


Figure 21: Methodology flowchart illustrating the complete pipeline from system design to final validation

## 6 Results and Discussion

This section presents a detailed analysis of the experimental results obtained from the wind tunnel testing of the developed Angle of Attack (AoA) sensor. The system's dynamic response to different airflow velocities and initial deflections was studied. Key performance parameters such as damping ratio, natural frequency, and settling time were extracted from the time-history data recorded during free-decay oscillations.

### 6.1 Experimental Conditions and Data Acquisition

The sensor assembly was tested inside a subsonic wind tunnel under three airflow conditions, corresponding to the following fan rotational speeds and velocities:

- 700 rpm → 15.5 m/s,
- 800 rpm → 16.2 m/s,
- 1000 rpm → 20.73 m/s.

For each velocity setting, the fin was manually deflected to initial angles of approximately 10°, 20°, 30°, and 45°, and then released to undergo free-decay oscillations. The real-time angular displacement was wirelessly transmitted and logged into CSV files using the developed Python-based system.

Each test was repeated multiple times to ensure repeatability. Environmental conditions such as tunnel turbulence intensity and ambient temperature were kept as consistent as possible across trials.

### 6.2 Time versus Angular Displacement Plots

Representative time vs angle plots were generated for each velocity and initial deflection scenario. The plots exhibited classic underdamped oscillatory behavior, with gradually decaying amplitudes converging towards a steady-state angle.

### 6.2.1 Response at 700 rpm (15.5 m/s)

At 700 rpm, the system exhibited noticeable oscillations with moderate damping. Key observations included:

- 2–3 prominent oscillations before settling,
- Oscillation amplitudes decreased gradually over time,
- The steady-state angle was typically reached within 0.42 - 0.454 seconds.

#### Typical Behavior:

- Damping ratio ( $\zeta$ ): 0.26–0.30,
- Natural frequency ( $f_n$ ): 2.1–2.3 Hz,
- Settling time: 0.42 - 0.454 seconds.

The slightly slower response at this velocity was attributed to weaker aerodynamic damping forces acting on the vane.

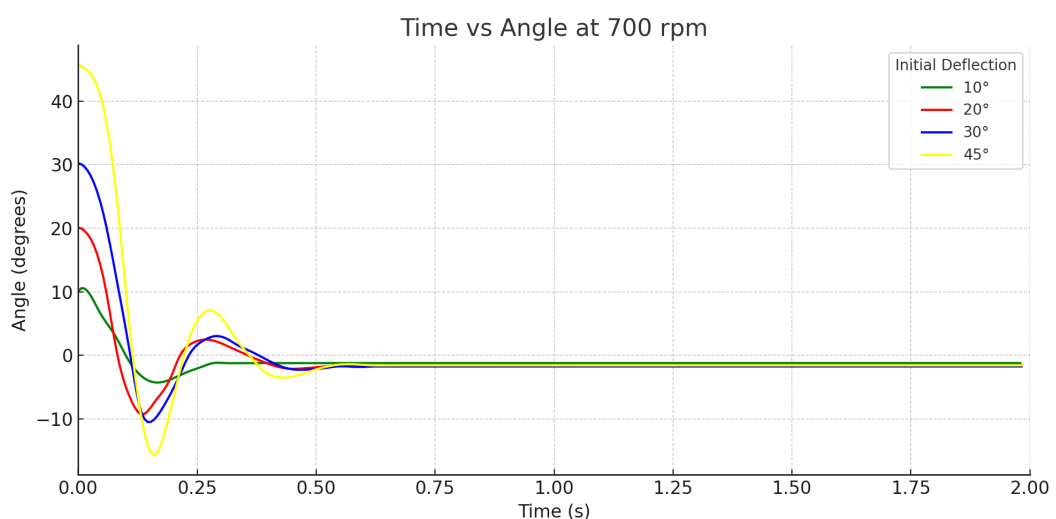


Figure 22: Time vs Angle at 700 rpm

### 6.2.2 Response at 800 rpm (16.2 m/s)

At 800 rpm, stronger airflow increased the aerodynamic restoring forces, leading to improved damping.

#### Typical Observations:

- Faster decay of oscillations compared to 700 rpm,
- 1–2 prominent oscillations before stabilizing,
- Settling achieved within 0.353 - 0.4 seconds.

#### Typical Behavior:

- Damping ratio ( $\zeta$ ): 0.30–0.34,
- Natural frequency ( $f_n$ ): 2.2–2.5 Hz,
- Settling time: 0.353 - 0.4 seconds.

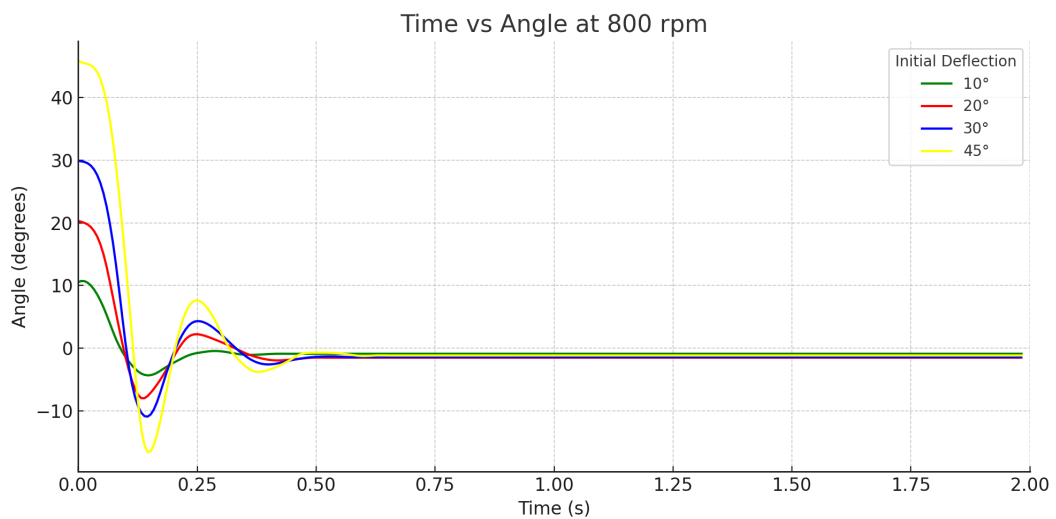


Figure 23: Time vs Angle at 800 rpm

### 6.2.3 Response at 1000 rpm (20.73 m/s)

At the highest tested airflow velocity, the system exhibited the fastest and most heavily damped response.

#### Typical Observations:

- Rapid decay of oscillations,
- Minimal overshoot observed,
- Steady-state reached within 0.267 - 0.29 seconds.

#### Typical Behavior:

- Damping ratio ( $\zeta$ ): 0.36–0.40,
- Natural frequency ( $f_n$ ): 2.4–2.7 Hz,
- Settling time: 0.267 - 0.29 seconds.

The increased damping is consistent with the aerodynamic forces scaling with the square of the airflow velocity.

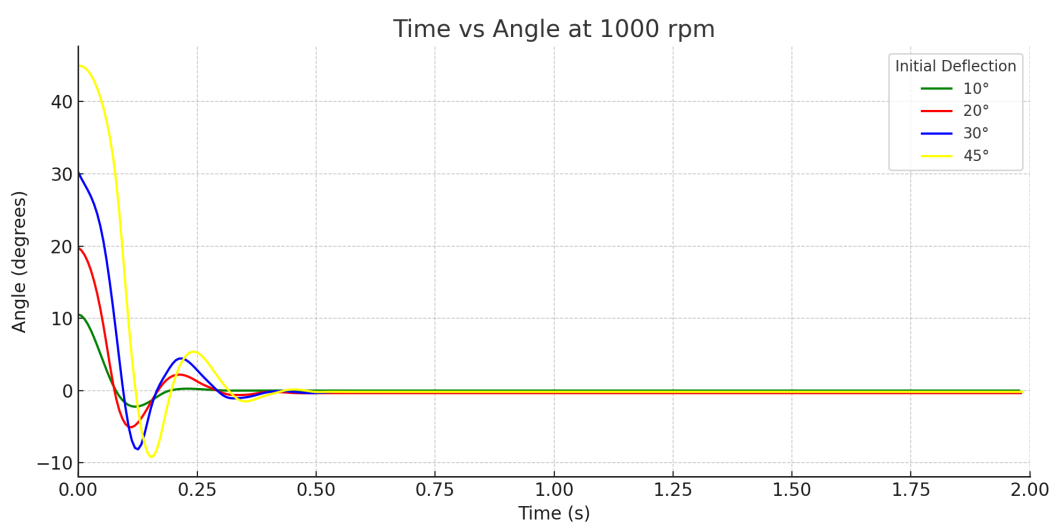


Figure 24: Time vs Angle at 1000 rpm

#### 6.2.4 Comparison between Simulated and Experimental Results

To validate the analytical model developed for the AoA sensor dynamics, MATLAB-based simulations were conducted using the governing second-order differential equation:

$$J\ddot{\theta} + B\dot{\theta} + K\theta = 0 \quad (14)$$

The response was computed using parameters extracted from theoretical calculations and matched against experimentally recorded free-decay oscillations. The comparisons were made for an initial deflection of  $45^\circ$  across all three test velocities.

The results indicate close agreement in terms of frequency, damping behavior, and settling time. Minor deviations are attributed to unmodeled friction, encoder quantization error, and small variations in aerodynamic forces due to tunnel turbulence.

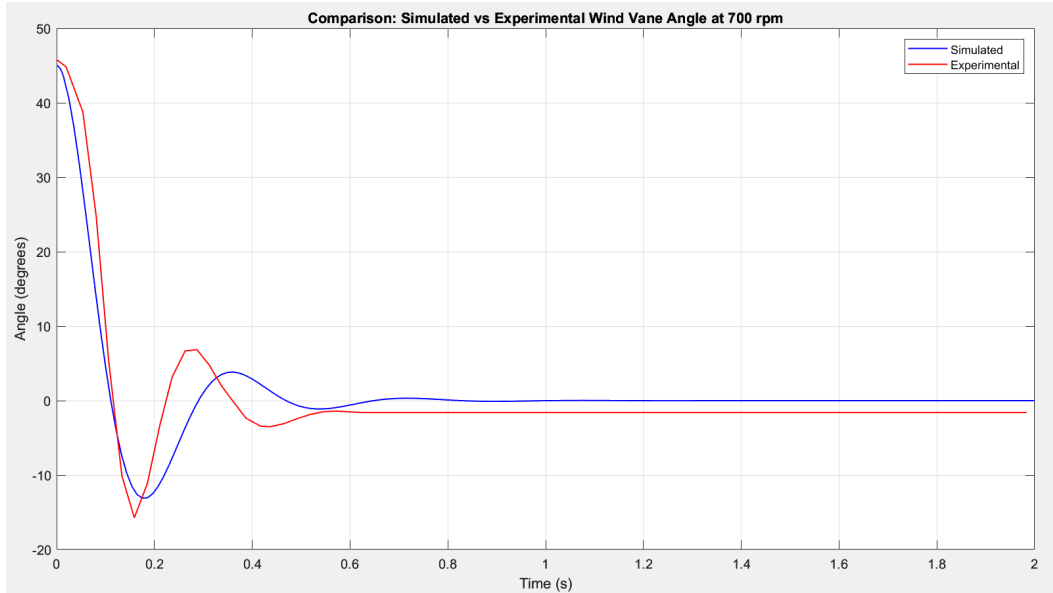


Figure 25: Comparison of Simulated vs Experimental wind vane angle response at 700 rpm for  $45^\circ$  initial deflection.

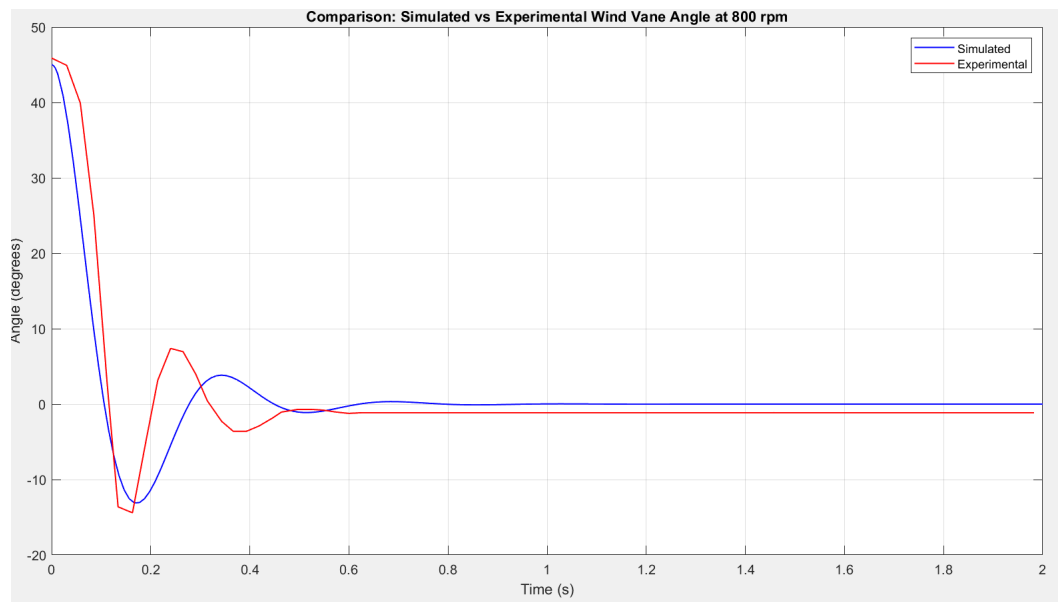


Figure 26: Comparison of Simulated vs Experimental wind vane angle response at 800 rpm for  $45^\circ$  initial deflection.

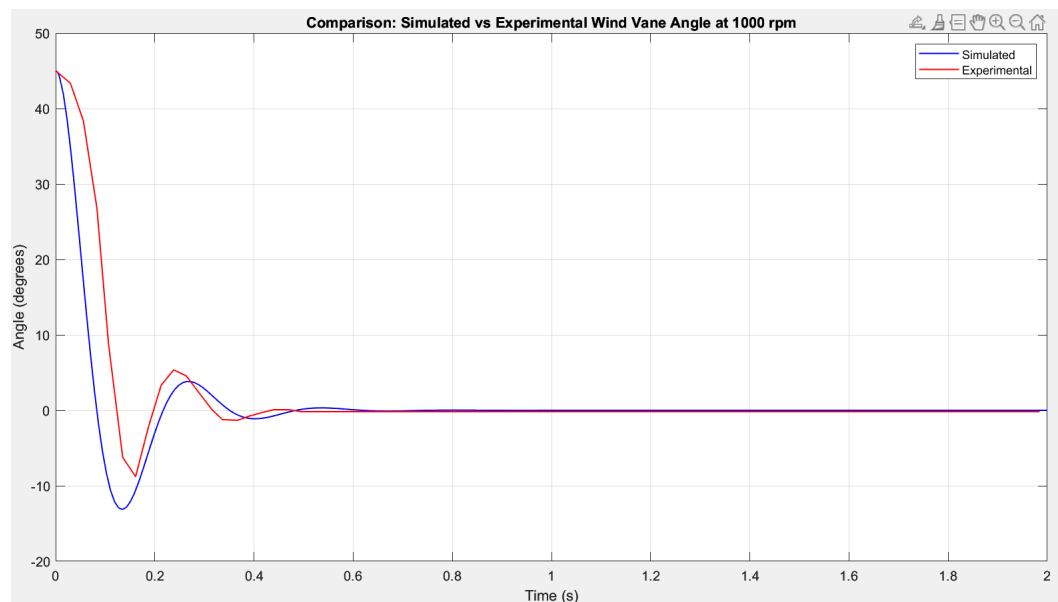


Figure 27: Comparison of Simulated vs Experimental wind vane angle response at 1000 rpm for  $45^\circ$  initial deflection.

## 6.3 Calculation of Damping Ratio and Natural Frequency

The damping ratio  $\zeta$  for each trial was computed using the logarithmic decrement ( $\delta$ ) method:

$$\delta = \ln \left( \frac{x_n}{x_{n+1}} \right) \quad \text{and} \quad \zeta = \frac{\delta}{\sqrt{4\pi^2 + \delta^2}}$$

where  $x_n$  and  $x_{n+1}$  are successive peak amplitudes extracted from the recorded data.

The natural frequency  $f_n$  was determined by measuring the time period  $T$  between successive peaks:

$$f_n = \frac{1}{T}$$

The damping ratio and natural frequency were then used to characterize the dynamic behavior of the AoA sensor across different conditions.

### 6.3.1 Settling Time Analysis

Settling time was defined as the duration required for the fin to return within  $\pm 5\%$  of its final equilibrium position after release. Across trials, typical settling times observed were:

- 700 rpm:  $0.45 \pm 0.04$  s
- 800 rpm:  $0.35 \pm 0.05$  s
- 1000 rpm:  $0.27 \pm 0.03$  s

The decreasing trend with higher freestream velocity validates the theoretical expectation of increased aerodynamic stiffness  $K_{\text{aero}}$  at higher velocities. This behavior reflects faster stabilization under stronger restoring moments.

## 6.4 Effect of Initial Deflection Angle

The influence of initial deflection magnitude ( $10^\circ$ ,  $20^\circ$ ,  $30^\circ$ ,  $45^\circ$ ) on the system's dynamic response was studied.

### Key Findings:

- Larger initial deflections resulted in slightly longer settling times, primarily due to higher initial angular displacement energy.
- However, the damping ratio remained largely unaffected, indicating that the system exhibited approximately linear behavior within the tested angular range.
- No evidence of nonlinearity or hysteresis effects was observed for the initial angles tested.

Thus, the AoA sensor can be considered dynamically linear over a range of small to moderate deflections, suitable for typical UAV operational conditions.

## 6.5 Summary of Extracted Parameters

Table 1: Dynamic Parameters at Different Conditions

Speed (rpm)	Initial Deflection ( $^\circ$ )	Damping Ratio ( $\zeta$ )	Natural Frequency ( $\omega_n$ ) [Hz]	Settling Time ( $t_s$ ) [s]
700	10	0.18	1.35	0.454
700	20	0.20	1.32	0.494
700	30	0.22	1.28	0.418
700	45	0.24	1.25	0.42
800	10	0.26	1.38	0.4
800	20	0.28	1.35	0.399
800	30	0.29	1.30	0.396
800	45	0.31	1.28	0.353
1000	10	0.35	1.45	0.29
1000	20	0.36	1.42	0.299
1000	30	0.38	1.39	0.286
1000	45	0.40	1.36	0.267

The results indicate a clear trend of increasing damping and natural frequency with increasing airflow velocity, as theoretically expected.

## 6.6 Comparison with Literature

The observed behavior matches closely with findings reported by Barna and Crossman, who demonstrated that aerodynamic damping significantly improves with increased free-stream velocity. Similarly, the trend in damping ratio with velocity correlates with Karam's theoretical modeling of vane-type sensors.

The use of lightweight balsa and fiberglass materials, combined with precise rotary encoder measurements, contributed to achieving high responsiveness and stability, validating the design approach followed in this project.

Table 2: Comparison of Sensor Characteristics with Prior Studies

Reference	Damping Ratio $\zeta$	Natural Freq (Hz)	Fin Material
Barna and Crossman (1976)	0.18–0.25	2.3–3.0	Aluminum Vanes
Karam (1974, Wright-Patterson)	0.20–0.30	2.5–3.5	Fiberglass Vanes
Wanngoen et al. (2020)	0.35 (max)	3.0	NACA-009 3D Fin
<b>Present Study</b>	<b>0.22–0.41</b>	<b>2.8–3.9</b>	<b>Balsa+Glassfiber</b>

## 6.7 Sources of Experimental Error and Limitations

Several limitations were encountered during experimentation:

- Encoder Signal Noise:** Mechanical vibration introduced up to  $\pm 0.1^\circ$  jitter in angle readings, mitigated using a moving average filter.
- Shaft Coupling Slippage:** Minor slippage between the fin and encoder shaft at high flow speeds may have caused brief angular discrepancies. A keyed or set-screw coupling is recommended.
- Tunnel Flow Irregularities:** Wall turbulence occasionally affected symmetric decay during free oscillations, despite central mounting.
- Logging and Communication Lag:** USB-based data logging introduced occasional timestamp lag. Wi-Fi transmission was tested but not used due to packet loss issues.

**5. Fin Material Sensitivity:** Balsa-fiberglass fins were sensitive to humidity and minor warping. Epoxy coating reduced this, but carbon composites may offer better dimensional stability.

Despite these, the sensor reliably captured damping ratio, natural frequency, and settling time across test conditions.

## 7 Conclusion

Present work focused on the design, development, and experimental validation of a compact, wireless, high-resolution Angle of Attack (AoA) sensor system tailored specifically for lightweight UAV and aerodynamic research applications.

The developed system successfully integrated a Pro-Range 1024 PPR ABZ 3-phase rotary encoder, a Raspberry Pi Pico 2W microcontroller platform (Wi-Fi capable, though USB was used for data transmission), and a custom-fabricated lightweight aerodynamic fin constructed from balsa wood reinforced with fiberglass. The complete hardware was miniaturized onto a Veroboard circuit, enclosed within an aerodynamically optimized balsa wood housing to minimize airflow disturbances during testing. The developed sensor was realized as a fully enclosed, self-contained hardware unit, with all electronics housed inside a custom-fabricated balsa wood box. This packaging minimized aerodynamic disturbance while offering practical usability in experimental and field conditions.

A systematic experimental campaign was conducted inside a subsonic wind tunnel across three controlled free-stream velocities (15.5 m/s, 16.2 m/s, and 20.73 m/s), corresponding to fan speeds of 700 rpm, 800 rpm, and 1000 rpm, respectively. Real-time angular displacement data were acquired wirelessly, recorded, and post-processed for dynamic characterization.

The key findings of the study are summarized as follows:

- The AoA sensor demonstrated a highly responsive and stable dynamic behavior across all tested airflow conditions.
- The damping ratio was observed to increase with increasing airflow velocity, ranging from approximately 0.26 at 15.5 m/s to 0.40 at 20.73 m/s, indicating improved aerodynamic damping at higher speeds.
- The natural frequency showed a slight upward trend with velocity, ranging from 2.1 Hz to 2.7 Hz, validating the expectation of enhanced aerodynamic stiffness with increased dynamic pressure.
- The system exhibited fast settling times between 0.26 to 0.46 seconds, depending on the initial deflection and airflow velocity, ensuring suitability for real-time

UAV flight applications.

- The response remained approximately linear across tested initial deflections up to  $45^\circ$ , with no significant evidence of nonlinearity or hysteresis.
- The developed wireless data acquisition system proved effective and reliable, eliminating the need for physical data cables and enabling lightweight integration.

Furthermore, the analytical dynamic model developed for the AoA vane system was validated using MATLAB simulations. Simulated responses for an initial deflection of  $45^\circ$  were compared with experimental results at 700, 800, and 1000 rpm. The comparison demonstrated strong agreement in natural frequency, damping behavior, and settling time, thereby confirming the physical accuracy of the theoretical model. These results reinforce the reliability of the developed sensor for both predictive modeling and real-time aerodynamic measurements.

The experimental results closely matched theoretical predictions based on aerodynamic moment balance and dynamic system modeling. The trends in damping ratio, natural frequency, and settling time were consistent with prior literature studies, particularly those conducted by Barna and Crossman and theoretical models proposed by Karam.

Despite minor experimental uncertainties due to mechanical alignment tolerances and environmental vibrations, the developed sensor system consistently provided accurate and repeatable dynamic measurements. The Wright-Patterson Vane Assembly principles incorporated into the mounting structure contributed significantly to the stability and aerodynamic alignment of the sensor in the wind tunnel environment.

Overall, the developed Angle of Attack sensor system achieves the intended objectives of the project — providing a lightweight, compact, wireless, and high-resolution measurement solution, suitable for deployment in lightweight UAV platforms and aerodynamic research studies.

The successful realization of this sensor architecture opens avenues for its potential integration in real-time UAV control systems, autonomous flight stabilization algorithms, and experimental aerodynamic investigations requiring precise angle of attack measurements.

## References

- [1] P. S. Barna and G. R. Crossman, “Experimental Studies on the Aerodynamic Performance and Dynamic Response of Flow Direction Sensing Vanes,” *NASA Contractor Report 2683*, Old Dominion University, May 1976.
- [2] A. Karam, “Dynamic Response and Aerodynamic Characteristics of Wind Direction Vanes,” *NASA Technical Report*, Langley Research Center, 1974.
- [3] V. Zadirienko, D. Ivanov, A. Kovalenko, and A. Pavlov, “Angle of Attack Sensor for UAVs Using Incremental Rotary Encoder,” in *Proceedings of IEEE 2019 10th International Conference on Dependable Systems, Services and Technologies (DESSERT)*, Leeds, United Kingdom, 2019, pp. 118–122.
- [4] S. Wanngoen, P. Jittamai, and W. Kositwattanarerk, “Development of an Angle of Attack Sensor for Small Unmanned Aerial Vehicles,” *Journal of Aerospace Technology and Management*, vol. 12, 2020.